Applied Catalysis B: Environmental 88 (2009) 550–556

Contents lists available at ScienceDirect

Applied Catalysis B: Environmental

journal homepage: www.elsevier.com/locate/apcatb

Catalytic oxidation of ethyl acetate over a cesium modified cryptomelane catalyst

V.P. Santos, M.F.R. Pereira, J.J.M. Órfão, J.L. Figueiredo *

Laboratório de Catálise e Materiais (LCM), Laboratório Associado LSRE/LCM, Departamento de Engenharia Química, Faculdade de Engenharia, Universidade do Porto, Rua Dr. Roberto Frias, 4200-465 Porto, Portugal

ARTICLE INFO

Article history:
Received 29 July 2008
Received in revised form 7 October 2008
Accepted 12 October 2008
Available online 1 November 2008

Keywords:
Ethyl acetate
Oxidation
Cryptomelane
Cesium
Basicity

ABSTRACT

Cryptomelane-type manganese oxide was synthesized by redox reaction under acid and reflux conditions. Cesium was incorporated into the tunnel structure by the ion-exchange technique. The catalytic oxidation of ethyl acetate in low concentration (1600 ppmv) was used to test the performance of the catalysts prepared. The presence of small amounts of cesium was found to improve the catalytic performance of cryptomelane. This behaviour was correlated with the basic properties of the catalyst. Temperature programmed experiments, and tests without oxygen in the feed, suggest that lattice oxygen atoms can react with ethyl acetate at low temperatures and are involved in the mechanism of ethyl acetate oxidation.

1. Introduction

Increasing concern about environmental and health effects resulting from emission of volatile organic compounds (VOC) has led to more stringent regulation standards, which require efficient and economic methods for VOC abatement [1]. Among the various methods that can be applied to efficiently control VOC emissions, catalytic oxidation seems to be the most efficient and cost-effective technology [2–4]. Catalyst formulation plays a key role towards the performance of the process.

Manganese oxides (β-MnO_2, γ-MnO_2, Mn_2O_3, Mn_3O_4) have been extensively studied as catalytic materials in the oxidation of many pollutants such as ethanol, acetone, propane and propene, ethyl acetate and CO [5–9]. Although the nature of the active sites for catalytic oxidation is not well established, several authors attribute their high catalytic activity to the mixed valence of framework manganese, and to the high mobility of oxygen species, implying the participation of the lattice oxygen in the reaction [10,11]. Among the various manganese oxides studied, microporous manganese oxides with hollandite structure (cryptomelane, OMS-2) have received appreciable attention for over 50 years, due to their exceptional catalytic properties and their shape-selective character [11–13]. Cryptomelane is a type of manganese oxide composed of 2×2 edge shared MnO_6 octahedral chains, which are corner connected to form one-dimensional tunnels (0.46 nm × 0.46 nm). Manganese in the octahedra is mainly present as Mn(IV) and Mn(III), and cations such as K^+ and small amounts of water partially occupy the tunnel to provide charge balance and stabilize the tunnel structure [14,15]. In order to further improve the electronic and catalytic properties, other metal cations have been introduced inside the tunnels or into the framework, by subsequent ion-exchange [16–20] or by substitution during synthesis [21–23]. The introduction of alkali metal into the tunnel can significantly modify the physical and chemical properties of cryptomelane, specially the surface acid–base properties [16]. Liu et al. [20] synthesized for the first time manganese oxides with Li^+, Na^+, Rb^+ as tunnel cations and found that the nature of the cation greatly influences the catalytic properties of OMS-2 towards total oxidation of cyclohexanol. Moreover, octahedral molecular sieves with Co^{2+}, Ag^+ and Cu^{2+} as tunnel cations showed high catalytic activities for CO oxidation at low temperatures [24,25].

The effect of cesium cations on the catalytic activity of cryptomelane for the oxidation of ethyl acetate was the subject of this study. It was expected that the presence of cesium into the tunnel structure of crytpomelane would change the surface acid–base properties and improve catalytic performance. A positive effect of alkali doping has been observed by several researchers in various systems [19,26,27] and has been related to the basic and acid surface properties of the catalyst and with the possible creation of new reaction pathways.

* Corresponding author. Tel.: +351 22 508 1663; fax: +351 22 508 1449.
E-mail addresses: santos.vera@fe.up.pt (V.P. Santos), fpereira@fe.up.pt (M.F.R. Pereira), jjmo@fe.up.pt (J.J.M. Órfão), jlfig@fe.up.pt (J.L. Figueiredo).

0926-3373/$ – see front matter © 2008 Elsevier B.V. All rights reserved.
doi:10.1016/j.apcatb.2008.10.006

2. Experimental

2.1. Synthesis

Cryptomelane-type manganese oxide (K-OMS-2) was synthesized using the reflux approach in acidic medium [12]. Cesium was incorporated into the tunnel structure by ion-exchange (sample Cs,K-OMS-2): 1 g of cryptomelane was stirred with 30 mL of 0.5 M solution of $CsNO_3$ (Aldrich) for 24 h. Every 4 h a fresh solution was added to improve the ion-exchange process. The solid obtained was filtered and washed with distilled water, followed by drying at 100 °C and calcination at 450 °C in air for 4.5 h.

2.2. Characterization

The structure, morphology, composition and texture of all samples were characterized by X-ray diffraction (XRD), scanning electron microscopy (SEM), inductively coupled plasma atomic emission spectroscopy (ICP-AES) and nitrogen adsorption, respectively. The thermal stability was studied by thermogravimetric analysis (TGA) under nitrogen atmosphere and temperature programmed desorption/mass spectroscopy (TPD/MS) under helium atmosphere. The average oxidation state of manganese and the basicity of O_2^- sites were determined by X-ray photoelectron spectroscopy (XPS).

2.2.1. Structure and morphology

The structure and phase purity of the prepared materials were analysed by X-ray diffraction using a PANalytical ŃPert PRO diffractometer with Cu Kα radiation source (λ = 0.154 nm) and with a beam voltage of 50 kV and 40 mA of beam current. The data were collected in the 2θ range of 10–100° with a scanning rate of 0.017°/s. The morphology of the materials was studied by field emission scanning electron microscopy (FEG-ESEM) on a FEI Quanta 400FEG/EDAX Genesis X4 M with a Schottky Emitter at an accelerating voltage of 10 kV.

2.2.2. Chemical composition

Manganese analyses were performed by inductively coupled plasma spectroscopy on a Plasma Perkin-Elmer Optima 2000 DV, while the potassium and cesium analyses were performed by atomic emission spectroscopy on a Perkin-Elmer AAnalyst 300. Prior to the analysis about 20 mg of sample were dissolved into an *acqua regia* solution, and the mixture was then diluted with water.

2.2.3. N_2 adsorption at 77 K

Nitrogen adsorption isotherms at liquid nitrogen temperature were obtained with a Quantachrome Instruments Nova 4200e. The samples were previously degassed at 300 °C for 3 h.

2.2.4. Thermal stability

Thermogravimetric analysis was done on a Mettler TA 4000 system under air or nitrogen atmosphere. About 10 mg of sample were loaded into a ceramic sample holder and the temperature was raised to 900 °C at 10 °C/min. Thermal stability of the materials was also studied by temperature programmed desorption combined with a mass spectrometer (TPD–MS). These experiments were conducted on an Altamira Instruments (AMI 200) apparatus. 100 mg of sample were loaded in the reactor and placed inside the furnace. The sample was purged with helium for 1 h at room temperature followed by heating to 900 °C at 5 °C/min in the same atmosphere.

2.2.5. Average oxidation state and basicity of O_2^- sites

The average oxidation state of manganese in all materials was obtained by XPS. XPS analysis was performed with a VG Scientific ESCALAB 200A spectrometer using Al Kα radiation (1486.6 eV). Charging effects were corrected by adjusting the binding energy of C 1s to 284.6 eV.

2.3. Catalytic experiments

The catalytic oxidation of ethyl acetate was carried out under atmospheric pressure in a fixed-bed reactor from Autoclave Engineers (BTRS Jr). A feed gas with a VOC concentration of 1600 ppmv and a space velocity of 16,000 h^{-1} was used in standard tests. The catalyst sample (0.05 g) was diluted with glass spheres of the same size as the catalyst particles ($0.2 < \phi < 0.5$ mm) (the total catalyst bed length was about 2 cm). Prior to the reaction the catalyst was activated under air at 400 °C for 1 h.

The reaction temperature was raised by steps of 10 °C, from 160 to 220 °C. The reactor was maintained at each temperature for 30 min in order to obtain experimental values at steady state. The conversion of ethyl acetate (X) and the conversion into CO_2 (X_{CO_2}) were respectively calculated as $X = 1 - (F_{VOC}/F_{VOC,in})$ and $X_{CO_2} = F_{CO_2}/\nu F_{VOC,in}$, where F_{VOC} is the outlet molar flow rate of VOC at steady state, $F_{VOC,in}$ is the inlet molar flow rate of VOC, F_{CO_2} is the outlet molar flow rate of CO_2 at steady state and ν is the number of carbon atoms in the VOC molecule ($\nu = 4$).

The analytical system consisted of a gas chromatograph equipped with a flame ionization detector (FID) for the analysis of the organic compounds, and an online non-dispersive infrared (NDIR) analyzer for CO_2.

The carbonaceous compounds retained in the catalyst ("coke") were quantified by temperature programmed oxidation (TPO) and temperature programmed desorption (TPD) techniques.

Temperature programmed experiments were also conducted after adsorption of ethyl acetate at 40 °C from a nitrogen stream. After saturation, the catalyst was purged with helium and the experiment started. The temperature was increased at 10 °C/min to 500 °C. The products were analysed by MS.

3. Results and discussion

3.1. Characterization

Fig. 1 shows the XRD patterns for K-OMS-2 and Cs,K-OMS-2 materials. All the diffraction peaks correspond to the pure cryptomelane phase [28]. It was expected that the incorporation of cesium would increase the unit cell volume, due to the higher ionic radius of cesium compared to potassium cations, as reported by Nur et al. [29] for the incorporation of Ti^{4+}. The unit cell volumes were obtained by calculation of the cell parameters (a, b and c) assuming tetragonal geometry: $1/(d_{hkl})^2 = ((h^2 + k^2)/a^2) + (l^2/c^2)$, where $d_{h\,k\,l}$ is the interplanar distance and $h\,k\,l$ are the Miller indices. The lattice parameters were determined by selecting two diffractogram lines ($\theta = 12.7°$ (1 1 0) and $\theta = 37.5°$ (2 1 1)) and solving the equations. The unit cell volumes obtained for K-OMS-2 (274 $Å^3$) and Cs,K-OMS-2 (277 $Å^3$) confirm the incorporation of cesium.

The presence of cesium does not change the characteristic morphology of cryptomelane, showing very long nanofibers with diameters in the range 10–20 nm (Fig. 2).

The stability of the materials was evaluated by TGA and TPD/MS experiments; as can be observed in Fig. 3, the incorporation of cesium into the tunnel structure does not affect significantly the cryptomelane stability (both materials show a weight loss of about 11%). The first weight loss occurs in the range of 90–200 °C (about 1%, for both materials), and is due to physically adsorbed water, as

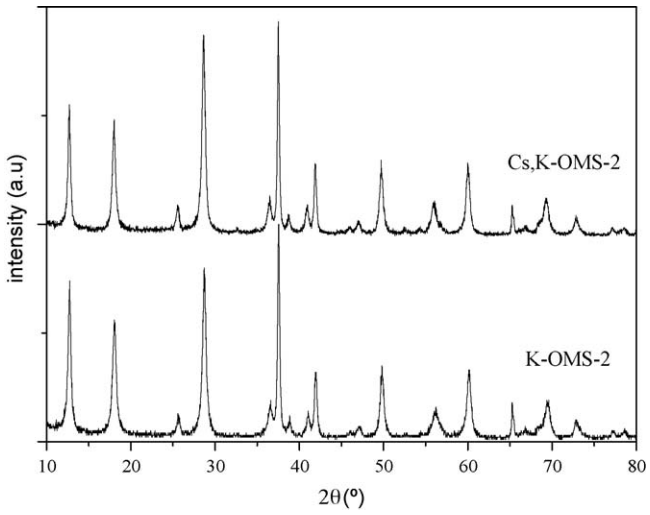

Fig. 1. XRD patterns of the K-OMS-2 and Cs,K-OMS-2 materials.

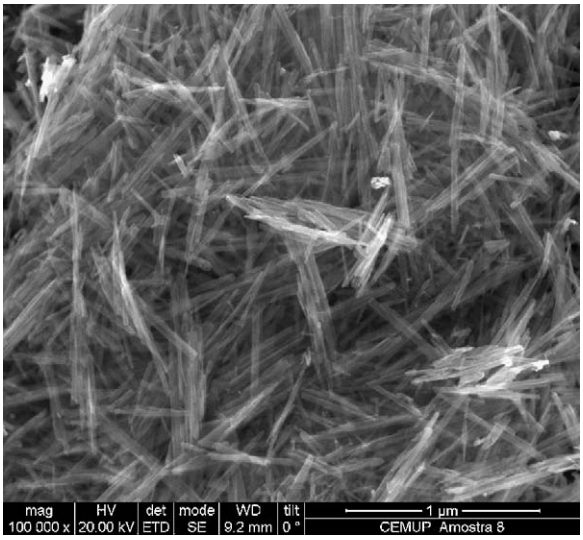

Fig. 2. SEM image of the K-OMS-2 material.

shown by TPD/MS analysis. Weight losses at higher temperatures (about 10%) are due to the evolution of oxygen species from the lattice, as confirmed by TPD/MS [30–32]. In nitrogen flow, the evolution of oxygen at temperatures higher than 500 °C promotes the decomposition of cryptomelane into Mn_2O_3 and then into Mn_3O_4 [33].

The average oxidation state of manganese (AOS) was obtained from the difference of binding energies between the Mn 3s peak and its satellite [34,35]. It is well known that for manganese oxides it is insufficient to employ the BE shifts of the Mn $2p_{3/2}$ to clearly distinguish the various manganese species (Mn(II), Mn(III) and Mn(IV)) [36]. As an alternative, Galakov et al. [34] showed that it is possible to obtain the manganese valence by studying the Mn 3s X-ray photoelectron spectra. The splitting of the 3s core-level X-ray photoemission spectra in transition metals and their compounds results from the exchange coupling between the 3s hole and the 3d electrons. The magnitude of the splitting is proportional to $(2S + 1)$, where S is the local spin of the 3d electrons in the ground state. This means that the binding energy for the 3s multiplet splitting of the manganese ion depends on the number of 3d electrons [34]. The same authors show that the energy difference (ΔE_s) between the main peak and its satellite decreases monotonically with the

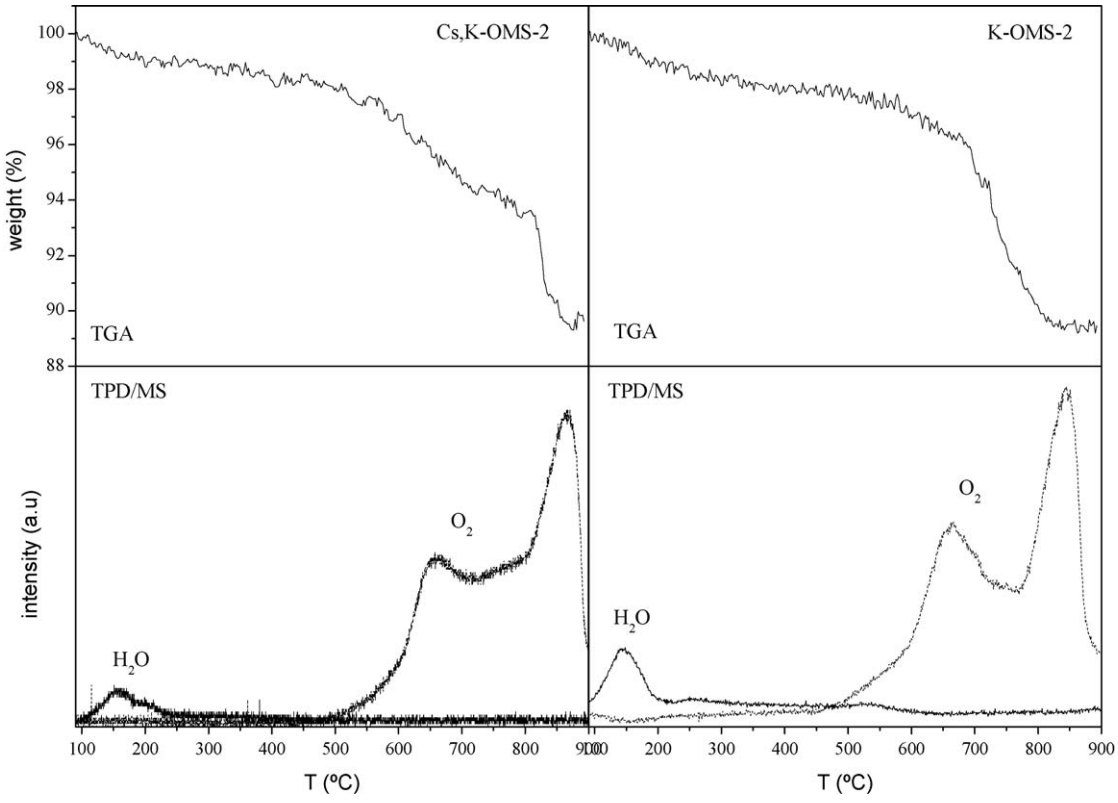

Fig. 3. TGA and TPD/MS experiments under nitrogen and helium, respectively.

Table 1
Properties of the catalysts.

Sample	Mn 3s ΔE_s (eV)	AOS	S_{BET} (m^2/g)	Chemical composition (ICP/AES)
K-OMS-2	4.50	3.89	45	$K_{0.12}MnO_2$
Cs,K-OMS-2	4.49	3.90	43	$K_{0.09}Cs_{0.03}MnO_2$

increase of the average oxidation state (AOS) of the manganese ions (except the region from Mn^{3+} to $Mn^{3.3+}$). The following relationship was obtained from the data in Ref. [34], which was used in the present work to calculate the AOS for both materials: AOS = $8.956 - 1.126\Delta E_s$ (eV). As can be seen in Table 1, the AOS of both materials is 3.9, which is in agreement with other authors [28]. This result suggests that Mn (IV) is dominant in both materials, and the influence of cesium incorporation on the average oxidation state of manganese is not significant.

The basic strength of the framework oxygen in all materials was also studied by XPS (Fig. 4). It is well known that there is a relationship between the O 1s binding energy determined by XPS and the intermediate electronegativities (S_{int}) [37]. The lower the O 1s BE, the lower is S_{int} (and the higher the basic strength) [38]. As can be seen in Fig. 4, the presence of cesium shifts the O 1s peak from 529.6 to 529.4 eV. This might indicate an increase of the catalyst surface basic strength. However, it should be mentioned that this difference is in the limit of the experimental error (±0.2 eV).

The bulk chemical compositions of both materials were determined by ICP/AES and are listed in Table 1. It may be observed that the bulk K/Mn atomic ratio in Cs,K-OMS-2 is lower than that of K-OMS-2, indicating a partial exchange with the cesium cations.

Relatively to the texture of the materials, it seems that the incorporation of cesium into the tunnel structure does not have a major influence in the surface area of the materials (see S_{BET} in Table 1).

3.2. Catalytic activities

The catalytic oxidation of ethyl acetate present in low concentration (1600 ppmv) was studied over K-OMS-2 and Cs,K-OMS-2 catalysts. The ethyl acetate conversion (X) and the conversion into CO_2 (X_{CO_2}), as a function of the reaction temperature, are shown in Fig. 5 for both catalysts.

Over the Cs,K-OMS-2 catalyst, the oxidation of ethyl acetate starts near 160 °C, reaching 100% conversion into CO_2 at 200 °C. With the K-OMS-2 catalyst, ethyl acetate oxidation starts at the same temperature, but complete oxidation into CO_2 and H_2O only occurs at a temperature 20 °C higher than that of the cesium dopped catalyst. The CO_2 selectivity (defined as X_{CO_2}/X) is not significantly affected by the presence of cesium. In both systems, the CO_2 selectivity was not 100% due to the formation of some oxygenated products: acetaldehyde was the major by-product detected, together with minor amounts of acetone. CO was never produced. Acetic acid, which could also be produced, could not be detected under the experimental conditions used.

In summary, it can be stated that the incorporation of cesium into the tunnel structure of cryptomelane improves the catalytic performance of this material.

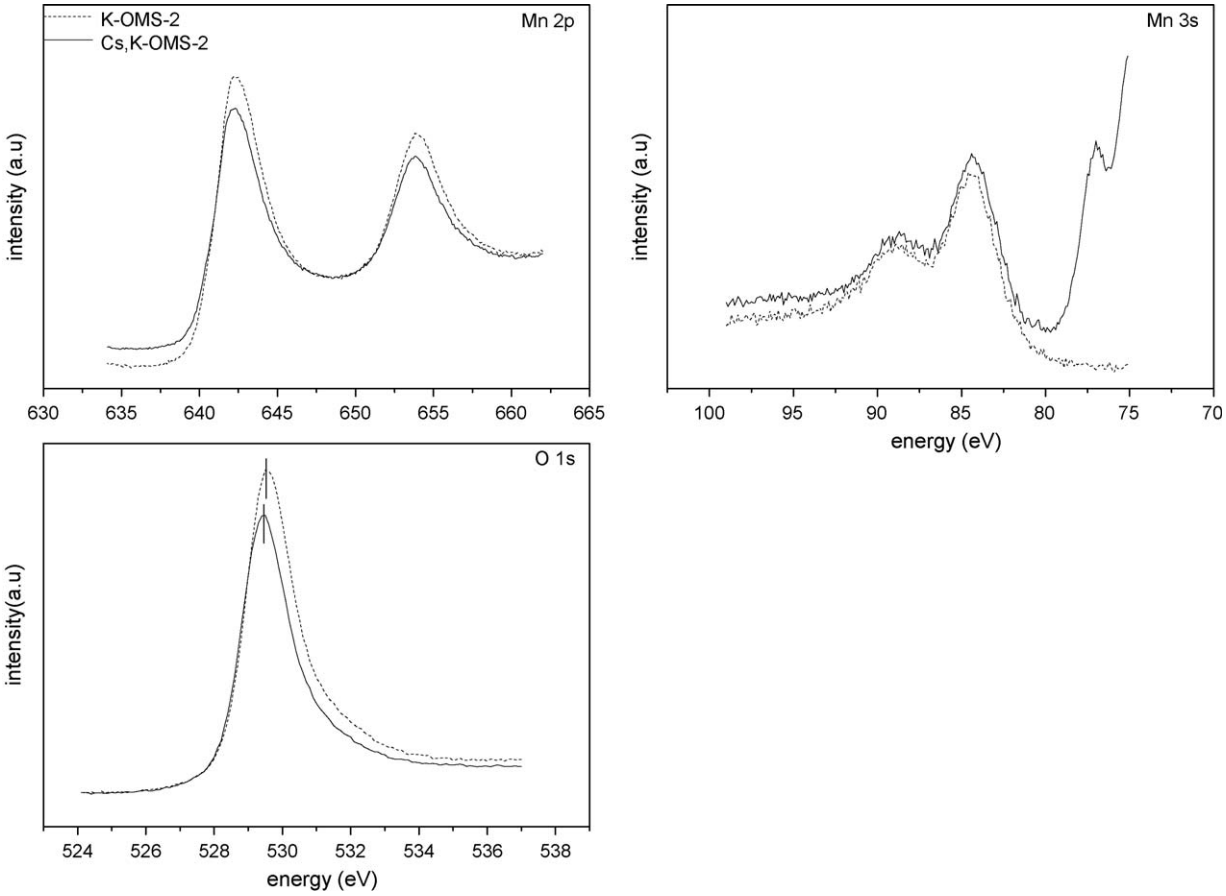

Fig. 4. Mn 2p, Mn 3s and O 1s XPS of the K-OMS-2 and Cs,K-OMS-2 samples.

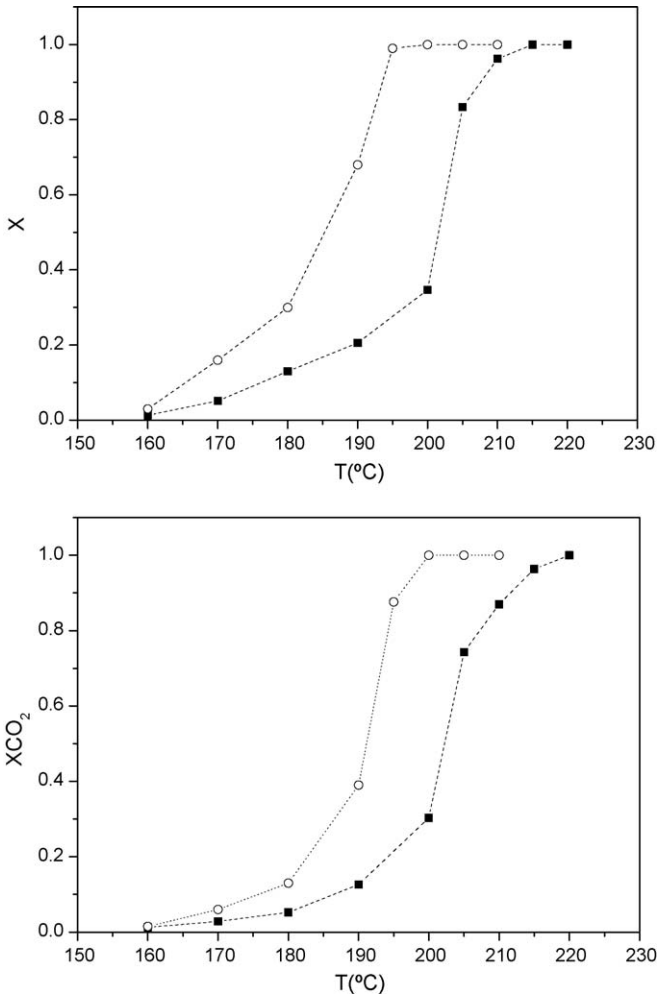

Fig. 5. Conversion of ethyl acetate (X) and conversion into CO_2 (X_{CO_2}) as a function of reaction temperature over catalysts K-OMS-2 (filled symbols) and Cs,K-OMS-2 (open symbols).

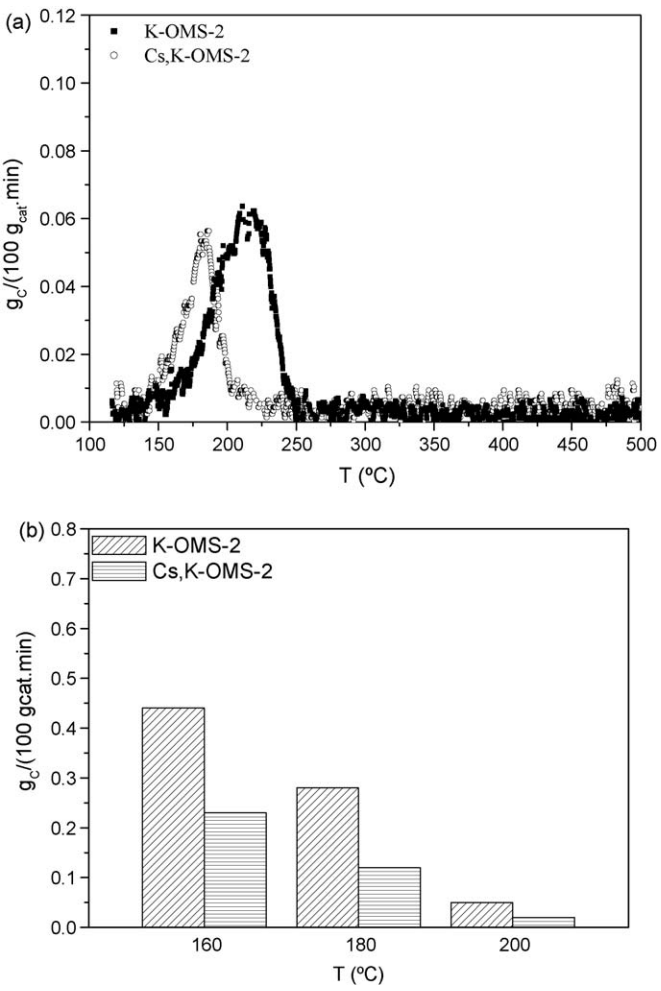

Fig. 6. (a) TPO curves after reaction at 160 °C over catalysts K-OMS-2 and Cs,K-OMS-2. (b) "Coke" content obtained by TPO after ethyl acetate oxidation at 160, 180 and 200 °C over catalysts K-OMS-2 and Cs,K-OMS-2.

The positive effect of alkali doping has also been observed by other authors in various reactions systems [19,26,27,39]. This effect has been ascribed to the basic and acid surface properties of the catalysts and with the possible creation of new reaction pathways. Gandía et al. [19] studied the catalytic oxidation of acetone and methyl-ethyl-ketone over Mn_2O_3 catalysts. They found that when this oxide is modified by alkali additives, like Na or Cs, the conversion is shifted to lower temperatures. They attributed this behaviour to the formation of strongly bound enolic species that can also undergo aldol condensation, producing compounds that remain adsorbed on the catalyst. The presence of Cs and Na favours the oxidation of these adsorbed species on the catalyst surface, reducing the combustion temperatures. The characterization results, namely the O 1s XPS spectrum of the two catalysts, might support this theory. As can be seen from Fig. 4, the presence of cesium shifts the binding energy to lower values, suggesting an increase in the surface basicity of the catalyst [27]. In order to analyse the effect of cesium on the oxidation of adsorbed species, TPO and TPD analyses were performed.

3.3. Temperature programmed experiments

The amount of adsorbed species deposited on the catalyst surface during the oxidation of ethyl acetate (generally designated as "coke") was measured by temperature programmed oxidation in air (TPO).

Fig. 6a shows the TPO profiles after 1 h reaction at 160 °C for K-OMS-2 and Cs,K-OMS-2 catalysts. A single peak was observed, with maximum at 214 and 180 °C, for K-OMS-2 and Cs,K-OMS-2, respectively. This result suggests that the presence of cesium renders the adsorbed products more reactive towards oxidation. Similar TPO profiles were obtained at 180 and 200 °C, only CO_2 being detected, in all cases.

Fig. 6b shows the carbon content after 1 h reaction at different temperatures (160, 180 and 200 °C), determined by integration of the TPO curves. It may be observed that the amount of adsorbed species in both catalysts decreases as the temperature increases.

Some TPO experiments were also performed in the K-OMS-2 catalyst, after stopping the reaction (180 °C) at different times: 5, 30, 60 min and 15 h, in order to analyse the evolution of the adsorbed species. It was observed that the carbon content remained constant after 30 min of reaction. This means that the net amount of retained compounds at steady state is negligible, suggesting that the major part of it consists of adsorbed reactant. This behaviour is essential to promote the stability of manganese oxide for long duration runs.

Fig. 7 shows two profiles obtained after 1 h reaction at 180 °C with K-OMS-2, one in air (TPO) and the other in helium (TPD). Surprisingly, there was no desorption of ethyl acetate in the TPD experiment, only CO_2 being detected, with a peak at 300 °C; the corresponding TPO shows a peak at 245 °C. This suggests that

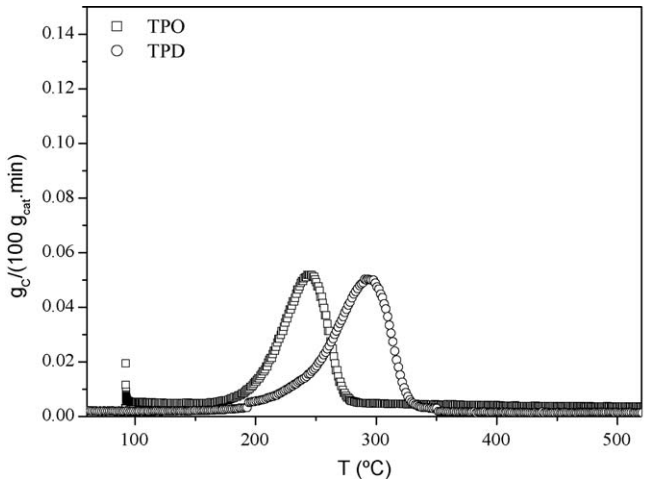

Fig. 7. Temperature programmed oxidation (TPO) and temperature programmed desorption (TPD) after reaction at 180 °C over the K-OMS-2 catalyst.

lattice oxygen is involved in the total oxidation of ethyl acetate. A similar behaviour was also observed in the oxidation of benzene and CO over cryptomelane [15].

In order to support this hypothesis, additional experiments in the absence of oxygen were made in both systems, namely a temperature programmed experiment (in helium) after adsorption of ethyl acetate at room temperature. The results obtained over both catalysts can be observed in Fig. 8. Desorption of ethyl acetate or other oxygenated products (such as ethanol, acetaldehyde, acetic acid and acetone) was not observed in this experiment, even at lower temperatures, which may indicate the absence of strong acid sites. The only products detected were H_2O and CO_2, probably formed during the oxidation of adsorbed ethyl acetate by lattice oxygen. Moreover, two peaks of CO_2 were detected in both systems, (237 and 304 °C, for K-OMS-2 catalyst and 209 and 290 °C for Cs,K-OMS-2 catalyst), which may indicate the presence of two types of adsorption sites. As can be observed, with the cesium modified catalyst the two CO_2 peaks were shifted to lower temperatures, confirming that cesium facilitates the oxidation of the adsorbed compounds.

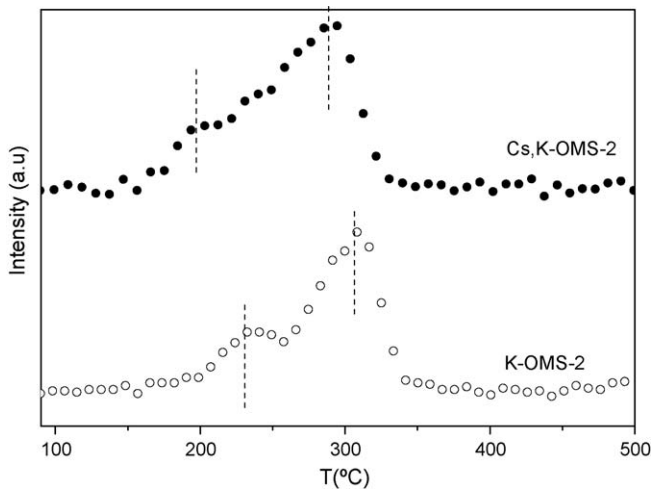

Fig. 8. Temperature programmed experiments (in helium) after adsorption of ethyl acetate at 40 °C over the K-OMS-2 and Cs,K-OMS-2 catalysts. The $m/z = 44$ signal is represented.

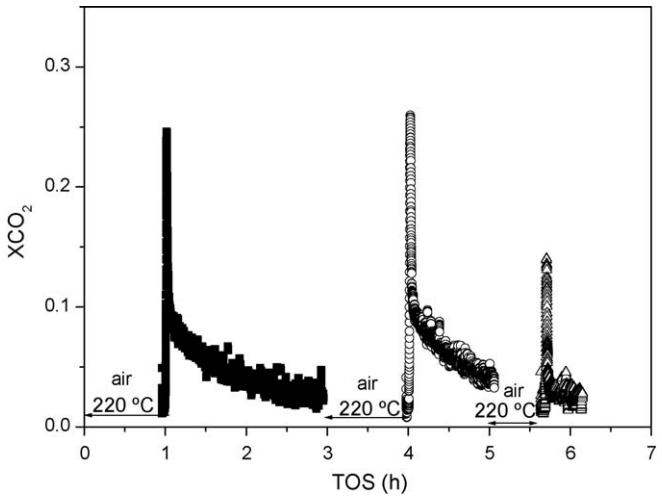

Fig. 9. Influence of the activation conditions on the conversion into CO_2 over catalyst K-OMS-2 at 220 °C without oxygen in the feed.

3.4. Reaction without oxygen in the feed

In order to study the effect of the lattice oxygen on the mechanism of ethyl acetate oxidation, successive tests over K-OMS-2 without oxygen in the feed were performed at 220 °C. In each cycle, prior to the reaction, the catalyst was activated in air at the reaction temperature. The activation time was 1 h in the first and second cycles, and 30 min in the third. The reactor was then purged with nitrogen in order to remove any oxygen physisorbed on the catalyst.

Fig. 9 shows the results of this experiment. It can be observed that the conversion into CO_2 sharply increases, reaching a maximum value and then decreases. The behaviour is the same in the first two cycles. In the third cycle, deactivation is faster. These results show that lattice oxygen species are involved in the mechanism of ethyl acetate oxidation, and that during the activation period there is an incorporation of oxygen into the catalyst lattice, which explains why the catalytic activity is recovered.

3.5. Stability experiments

The stability of the cesium modified catalyst was evaluated in long duration experiments. The conversion into CO_2 at 195 and

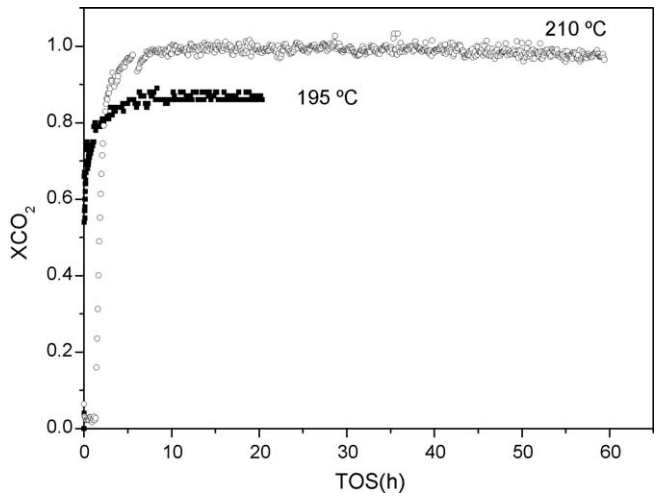

Fig. 10. Influence of time on stream (TOS) on the conversion into CO_2 over Cs,K-OMS-2 at 195 and 210 °C.

210 °C as a function of time on stream (TOS) is shown in Fig. 10. The histories of conversion into CO_2 are similar to those obtained by the light-off curves ($X_{CO_2} = 0.87$ and $X_{CO_2} = 1.0$ at 195 and 210 °C, respectively). It seems that there is no stabilization period and the conversion into CO_2 remains constant during the experiment. This result shows that the cesium modified catalyst is stable.

Some tests were also made in order to evaluate the performance of the catalyst after being used and treated in air up to 500 °C. It was observed that there was no deactivation after the regeneration treatments.

4. Conclusions

The following conclusions can be drawn from this study:

- K-OMS-2 is active for the oxidation of ethyl acetate into CO_2.
- The incorporation of cesium into the tunnel structure improves the performance of K-OMS-2 catalyst in the oxidation of ethyl acetate. This improvement may be correlated to the enhanced basic properties of the catalyst.
- The cesium modified cryptomelane catalyst is quite stable during long duration experiments.
- Lattice oxygen atoms are involved in the mechanism of ethyl acetate oxidation.

Acknowledgments

This work was supported by Fundação para a Ciência e a Tecnologia (FCT) and FEDER under Programme POCI/1181 and Project PTDC/AMB/69065/2006. V.P.S. acknowledges the grant received from FCT (SFRH/BD/23731/2005). The authors also acknowledge the Programme CYTED (PI0269), and Dr. Carlos M. Sá (CEMUP) for assistance with XPS analyses.

References

[1] R. Atkinson, Atmos. Environ. 34 (2000) 2063–2101.
[2] E.C. Moretti, N. Mukhopadhyay, Chem. Eng. Prog. 89 (1993) 20–26.
[3] E.N. Ruddy, L.A. Carroll, Chem. Eng. Prog. 89 (1993) 28–35.
[4] K. Everaert, J. Baeyens, J. Hazard. Mater. 109 (2004) 113–139.
[5] C. Lahousse, A. Bernier, P. Grange, B. Delmon, P. Papaefthimiou, T. Ioannides, X. Verykios, J. Catal. 178 (1998) 214–225.
[6] K.M. Parida, A. Samal, Appl. Catal. A: Gen. 182 (1999) 249–256.
[7] E. Finocchio, G. Busca, Catal. Today 70 (2001) 213–225.
[8] L. Lamaita, M.A. Peluso, J.E. Sambeth, H. Thomas, G. Mineli, P. Porta, Catal. Today 107–08 (2005) 133–138.
[9] L. Lamaita, M.A. Peluso, J.E. Sambeth, H.J. Thomas, Appl. Catal. B: Environ. 61 (2005) 114–119.
[10] C. Cellier, V. Ruaux, C. Lahousse, P. Grange, E.M. Gaigneaux, Catal. Today 117 (2006) 350–355.
[11] J. Luo, Q. Zhang, J. Garcia-Martinez, S.L. Suib, J. Am. Chem. Soc. 130 (2008) 3198–3207.
[12] J. Luo, Q. Zhang, A. Huang, S.L. Suib, Micropor. Mesopor. Mater. 35–36 (2000) 209–217.
[13] F.N. Aguero, A. Scian, B.P. Barbero, L.E. Cadus, Catal. Today 133–135 (2008) 493–501.
[14] S.L. Suib, Curr. Opin. Solid State Mater. Sci. 3 (1998) 63–70.
[15] S.L. Suib, J. Mater. Chem. 18 (2008) 1623–1631.
[16] Y.F. Shen, S.L. Suib, C.L. Oyoung, J. Am. Chem. Soc. 116 (1994) 11020–11029.
[17] Q. Feng, H. Kanoh, Y. Miyai, K. Ooi, Chem. Mater. 7 (1995) 148–153.
[18] J. Cai, J. Liu, W.S. Willis, S.L. Suib, Chem. Mater. 13 (2001) 2413–2422.
[19] L.M. Gandia, A. Gil, S.A. Korili, Appl. Catal. B: Environ. 33 (2001) 1–8.
[20] J. Liu, V. Makwana, J. Cai, S.L. Suib, M. Aindow, J. Phys. Chem. B 107 (2003) 9185–9194.
[21] X. Chen, Y.F. Shen, S.L. Suib, C.L. O'Young, J. Catal. 197 (2001) 292–302.
[22] J. Liu, Y.C. Son, J. Cai, X.F. Shen, S.L. Suib, M. Aindow, Chem. Mater. 16 (2004) 276–285.
[23] W. Gac, Appl. Catal. B: Environ. 75 (2007) 107–117.
[24] E. Nicolas-Tolentino, Z.R. Tian, H. Zhou, G.G. Xia, S.L. Suib, Chem. Mater. 11 (1999) 1733–1741.
[25] R. Hu, Y. Cheng, L. Xie, D. Wang, Chin. J. Catal. 28 (2007) 463–468.
[26] C.H. Lee, Y.W. Chen, Appl. Catal. B: Environ. 17 (1998) 279–291.
[27] J. Tsou, P. Magnoux, M. Guisnet, J.J.M. Orfao, J.L. Figueiredo, Appl. Catal. B: Environ. 51 (2004) 129–133.
[28] R.N. Deguzman, Y.F. Shen, E.J. Neth, S.L. Suib, C.L. Oyoung, S. Levine, J.M. Newsam, Chem. Mater. 6 (1994) 815–821.
[29] H. Nur, F. Hayati, H. Hamdan, Catal. Commun. 8 (2007) 2007–2011.
[30] Y.G. Yin, W.Q. Xu, R. Deguzman, S.L. Suib, C.L. Oyoung, Inorg. Chem. 33 (1994) 4384–4389.
[31] Y.G. Yin, W.Q. Xu, Y.F. Shen, S.L. Suib, C.L. Oyoung, Chem. Mater. 6 (1994) 1803–1808.
[32] Y.G. Yin, W.Q. Xu, S.L. Suib, C.L. Oyoung, Inorg. Chem. 34 (1995) 4187–4193.
[33] D.L. Bish, J.E. Post, Am. Miner. 74 (1989) 177–186.
[34] V.R. Galakhov, M. Demeter, S. Bartkowski, M. Neumann, N.A. Ovechkina, E.Z. Kurmaev, N.I. Logachevskaya, Y.M. Mukovskii, J. Mitchell, D.L. Ederer, Phys. Rev. B 65 (2002) 4.
[35] I. Barrio, I. Legorburu, M. Montes, M.I. Dominguez, M.A. Centeno, J.A. Odriozola, Catal. Lett. 101 (2005) 151–157.
[36] M.L. Rojas, J.L.G. Fierro, L.G. Tejuca, A.T. Bell, J. Catal. 124 (1990) 41–51.
[37] J. Weitkamp, M. Hunger, U. Rymsa, Micropor. Mesopor. Mater. 48 (2001) 255–270.
[38] Y. Okamoto, M. Ogawa, A. Maezawa, T. Imanaka, J. Catal. 112 (1988) 427–436.
[39] C.A. Querini, L.M. Cornaglia, M.A. Ulla, E.E. Miro, Appl. Catal. B: Environ. 20 (1999) 165–177.